npj | Materials Degradation

www.nature.com/npjmatdeg

BRIEF COMMUNICATION OPEN

The hydrogen-induced pitting corrosion mechanism in duplex stainless steel studied by current-sensing atomic force microscopy

Vladislav Yakubov[1,2], Meichao Lin[1], Alex A. Volinsky[1,2], Lijie Qiao[1] and Liqiu Guo[1]

Duplex stainless steels have excellent corrosion resistance due to their two-phase microstructure and electrically insulating passive film. Nevertheless, hydrogen charging causes deterioration of the corrosion protection mechanisms, resulting in increased pitting susceptibility. In this study, current-sensing atomic force microscopy was used to investigate the electrical properties of the passive film formed on 2507 duplex stainless steel before hydrogen charging. Results were compared with optical images of pitting corrosion initiation after hydrogen charging and $FeCl_3$ exposure. Highest passive film conductivity and current density were seen at grain boundaries, indicating poor passive film development and high pitting probability. High conductivity was also observed on the passive film located at the adjacent austenite phase, alluding to favorable conditions for pitting corrosion propagation. Phases were identified by magnetic force microscopy, while pit initiation with subsequent propagation after hydrogen charging and $FeCl_3$ exposure was observed using optical microscopy. Pitting corrosion initiated at grain boundaries and propagated into the austenite grains. This study identified the pitting initiation and propagation mechanisms in 2507 duplex stainless steel.

npj Materials Degradation (2018)2:39 ; https://doi.org/10.1038/s41529-018-0062-1

INTRODUCTION

Stainless steels resist corrosion primarily due to a natural passive film formed on the surface.[1] However, the resistance of stainless steel to pitting corrosion is poor when the material is exposed to a chloride-containing environment.[2] Exposure of stainless steel to hydrogen is known to increase corrosion susceptibility, so much work has been done to determine the effects of hydrogen on pitting.[3–7] It was previously shown that hydrogen increases the surface activity of passive film and deteriorates passive film stability.[5–7] In a recent review, Thomas et al.[8] stated that hydrogen destabilizes the passive film by altering its chemical composition, thus changing the dielectric constant and the electronic properties of the passive film. However, the role of hydrogen in relation to the local electronic properties of passive film and pitting corrosion in stainless steel remains far from clarity.

It is known that corrosion failure of duplex stainless steels (DSS) often begins with pitting corrosion before subsequent stress corrosion cracking development in a chloride-containing environment.[9–14] Yao et al.[15] studied passive film behavior of hydrogen-charged 316 austenitic stainless steel and determined that hydrogen decreased the passive film breaking load, the Young's modulus, and the fracture stress, and reduced the cohesive strength between the stainless steel matrix and the passive film. However, it is difficult to characterize the electrical behavior of hydrogen-containing passive film on duplex stainless steel using traditional macroscopic measuring methods, such as electrochemical impedance spectroscopy and photoelectrochemical analysis, because duplex stainless steel has a heterogeneous structure composed of ferrite and austenite grains. This leads to differences in semiconductor characteristics of the passive film formed on the different phase grains and grain boundaries. Fortunately, current-sensing atomic force microscopy (CSAFM) can detect the hydrogen-induced local electrical properties' change of passive film on different areas of duplex stainless steel by acquiring the electrical conductivity.[16–18] In previous research,[18] we used CSAFM to characterize the semiconductor behavior of passive film on ferrite and austenite grains before and after hydrogen charging. However, the electrical behavior at grain boundaries was not investigated. In general, grain boundaries are more susceptible to pitting corrosion, especially in a hydrogen-containing environment. This is due to the grain boundaries containing more defects, making these areas preferentially gather hydrogen, which causes the subsequently formed passive film to have poor electrical properties.

Present work aims to use CSAFM current mapping and optical imaging to determine the performance of passive film formed on grain boundaries and different phase grains before and after hydrogen charging of duplex stainless steel. The more active areas of the passive film are identified as susceptible pitting initiation sites. This research furthers the understanding of the mechanisms of hydrogen-induced film breakdown and pitting corrosion in duplex stainless steel.

RESULTS AND DISCUSSION

Passive film conductivity

Fig. 1a illustrates the CSAFM map with 0.8 V applied tip bias of passive film formed before hydrogen charging. CSAFM

[1]Beijing Advanced Innovation Center for Material Genetic Engineering Key Laboratory for Environmental Fracture (MOE), University of Science andTechnology Beijing, Beijing 100083, China and [2]Department of Mechanical Engineering, University of South Florida, Tampa, FL 33620, USA
Correspondence: Alex A. Volinsky (volinsky@usf.edu) or Liqiu Guo (glq@mater.ustb.edu.cn)

Received: 13 July 2018 Revised: 5 November 2018 Accepted: 7 November 2018
Published online: 06 December 2018

Published in partnership with CSCP and USTB

npj nature partner journals

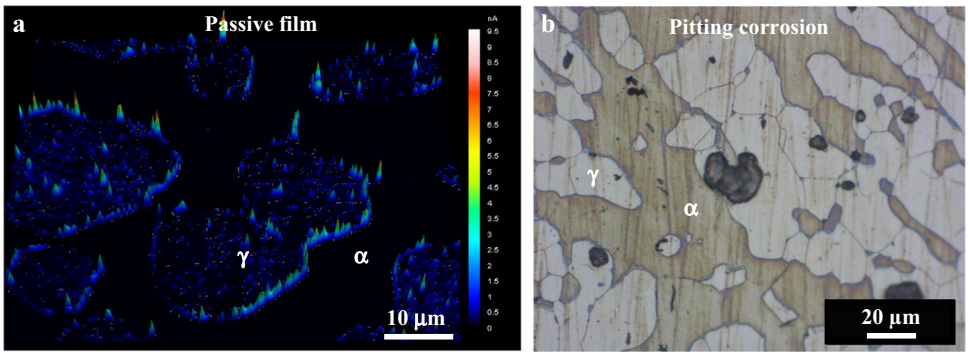

Fig. 1 **a** Current-sensing atomic force microscopy 3D current map of the air-formed passive film with high current sites at grain boundaries and the austenite phase; **b** Optical image showing pitting corrosion after hydrogen charging and $FeCl_3$ exposure

Table 1. Chemical composition in wt.% of 2507 duplex stainless steel for ferrite (α) and austenite (γ) phases

	C	Cr	Mn	Fe	Ni	Mo	N
α	0.011 ± 0.001	28.59 ± 0.17	0.66 ± 0.09	61.59 ± 0.31	5.06 ± 0.12	5.04 ± 0.07	0.06 ± 0.001
γ	0.012 ± 0.001	25.72 ± 0.16	0.81 ± 0.09	62.4 ± 0.31	7.15 ± 0.12	3.75 ± 0.06	0.59 ± 0.01

measurements were conducted in the air with 328 nN tip normal load to obtain a clear current map image, prevent film fracture and limit electron tunneling effects.[17,18] The ferrite and austenite phases can be identified in the CSAFM current maps based on our previous work.[17–19] In Fig. 1a, the passive film on grain boundaries exhibits much higher conductivity (brighter color) than passive film on either the ferrite or austenite grains. This is because the grain boundaries act as hydrogen trap sites, thus affecting interfacial processes occurring at the material's surface[8] and creating unfavorable conditions for the development of stable, insulating passive film. Moreover, the passive film on austenite grains shows higher conductivity (brighter color) than on ferrite grains (darker color), which means that passive film on ferrite grains is more insulating (more stable) than on austenite grains. The current measured during CSAFM is negatively correlated with the corrosion resistance of the scanned area. It can be said that areas of the passive film with high CSAFM-measured current also have high pitting susceptibility. The low conductivity on the ferrite grains is attributed to enriched chromium oxides in the passive film formed in these areas.[20] Current spikes in Fig. 1a are related to nanoscale defects present in the passive film. Figure 1b shows an optical image of pit initiation and propagation after hydrogen charging and $FeCl_3$ exposure. More hydrogen is adsorbed in the austenite grains than in the ferrite grains due to hydrogen having a higher solubility and a lower diffusivity in the face-centered cubic austenite phase compared with the body-centered cubic ferrite phase.[21,22] It can be concluded that hydrogen facilitates pitting corrosion initiation at grain boundaries and austenite grains, i.e. hydrogen makes the passive film less stable and more conductive.

It is generally accepted that pitting is a result of the localized breakdown of the passive film, which usually occurs at specific sites of low film stability.[23] In our previous research,[24] pitting of a hydrogen-charged specimen exposed to a 6% $FeCl_3$ solution initially occurred at the grain boundaries or at the austenite grains, and then appeared at the ferrite grains. Therefore, areas with poorly insulating passive film, such as grain boundaries and austenite grains, can be considered more susceptible to pitting corrosion. Pitting nucleation occurs at grain boundaries because these areas gather hydrogen preferentially, which causes the passive film to easily break down. Meanwhile, the vast majority of hydrogen gathers in the austenite grains, which can accelerate the breakdown of the passive film and cause pitting nucleation in this area. However, under the same hydrogen charging conditions, less hydrogen gathers in the ferrite grains, so pitting nucleation appears later here compared to other areas.

Passive film current density

Combining the contact area calculated by the Hertzian elastic contact formula with the current output of the CSAFM, yields the average current density of passive film at the grain boundaries and austenite grains of 0.074 nA/nm^2 and 0.003 nA/nm^2, respectively. The maximum current density at the grain boundaries and austenite grains is 0.109 nA/nm^2 and 0.077 nA/nm^2, respectively. Current flow is negligible on the ferrite grains, corresponding to black regions in Fig. 1a. Thus, it can also be deduced that pitting corrosion will preferentially begin at the grain boundaries or in the austenite phase of 2507 duplex stainless steel, which matches our previous results.[21,24,25]

CSAFM was used to directly observe the conductivity of passive film formed on grain boundaries, austenite and ferrite grains prior to hydrogen charging. The passive film on austenite grains and grain boundaries had much higher conductivity than on ferrite grains. Hydrogen charging was seen to cause an increase in corrosion susceptibility due to poor passive film formation, especially at grain boundaries and at austenite grains. This resulted in pitting corrosion initially occurring in these areas before spreading to ferrite grains after hydrogen charging and $FeCl_3$ solution exposure.

METHODS

Sample preparation

The material used for the experiment was commercially available 2507 duplex stainless steel with the composition shown in Table 1, as reported previously.[26] The specimen was machined into a square sheet with the dimensions of 10 × 10 × 0.7 mm. The specimen was prepared by first wet grinding with silicon carbide paper up to 2000 grit before mechanical polishing with 1.5 μm diamond paste. Final polishing with a solution of HNO_3:H_2O = 1:1 for 20 s at 1.2 V was performed to ensure that surface

stresses were eliminated. The specimen was then cleaned in ethanol, dried with nitrogen gas flow, and held at 25 °C in the air for 24 h to develop a native passive film. This treatment was performed to achieve a very smooth surface suitable for the CSAFM measurements. Hydrogen charging was performed at room temperature in 0.5 M H_2SO_4 aqueous solution with 0.25 g/L As_2O_3 added to increase hydrogen adsorption. A platinum electrode was used as the anode and the specimens acted as the cathode. The specimen was charged from all sides at 2.5 mA/cm^2 current density for 24 h. Then, the passive film was formed on the hydrogen-charged specimen with the same parameters as for the uncharged specimen.

Instrumentation

CSAFM measurements of the passive film before and after hydrogen charging were conducted in the air at 25 °C and 25% relative humidity using an Agilent 5500 AFM set to current-sensing mode and equipped with the DPE14/AIBS platinum-coated silicon tip (50 nm tip radius and 5.7 N/m force constant). The optimal tip normal load was determined to be 328 nN, which was found by bringing the CSAFM tip into contact with the sample surface. Then, the normal load was increased to a certain value and the I–V curve was recorded. After this, the tip was moved to a nearby unscanned area and the I–V curve was recorded with a higher tip normal load. Ten different normal loads were used. At the 328 nN tip normal load, a stable and reproducible I–V relationship was observed. The Hertzian equation neglects interfacial adhesion. Therefore, the error in the calculated contact area is larger at lower tip normal loads. At tip normal loads above 492 nN, the high tip pressure caused passive film deformation outside of the elastic range. This was determined by adding load and then observing if the measured current returned to original values after the additional load was removed. A tip bias was chosen based on the breakdown voltage of passive film and clarity of current maps at the 328 nN tip normal load.

The current density at the contact area

For current density calculations, it was necessary to determine the contact area of the CSAFM tip on the film surface. This was performed using the Hertzian elastic contact formula between a sphere and a flat plane,[27,28] as shown in Eq. 1.

$$A = \pi a^2 = \pi\left(\frac{3PR}{4E}\right)^{\frac{2}{3}}. \quad (1)$$

The effective Young's modulus, E, is calculated as shown in Eq. 2.

$$E = \left[\frac{\left(1-\nu_1^2\right)}{E_1} + \frac{\left(1-\nu_2^2\right)}{E_2}\right]^{-1}. \quad (2)$$

In these equations, A is the contact area, a is the contact radius, and E is the effective Young's modulus. R is the tip radius and P is the normal tip load, while ν_1, ν_2, and E_1, E_2 are the Poisson's ratio and Young's modulus of the tip and the specimen, respectively. For the materials used in this study, $\nu_1 = 0.28$, $\nu_2 = 0.3$, E_1=169 GPa, and E_2=200 GPa.

DATA AVAILABILITY

The data that support the findings in this paper are available from the corresponding authors upon reasonable request.

ACKNOWLEDGEMENTS

We acknowledge support from the National Natural Science Foundation of China (51431004 and 51571030) and from the National Science Foundation (IRES 1358088).

AUTHOR CONTRIBUTIONS

V.Y. wrote the manuscript, M.L. conducted the CSAFM measurements, A.A.V., L.Q. and L.G. designed the experiments, interpreted the data and corrected the manuscript. All authors contributed to writing the manuscript.

ADDITIONAL INFORMATION

Competing interests: The authors declare no competing interests.

Publisher's note: Springer Nature remains neutral with regard to jurisdictional claims in published maps and institutional affiliations.

REFERENCES

1. Souier, T., Martin, F., Bataillon, C. & Cousty, J. Local electrical characteristics of passive films formed on stainless steel surfaces by current sensing atomic force microscopy. *Appl. Surf. Sci.* **256**, 2434–2439 (2010).
2. Liou, H. Y., Hsieh, R. I. & Tsai, W. T. Microstructure and stress corrosion cracking in simulated heat-affected zones of duplex stainless steels. *Corros. Sci.* **44**, 2841–2856 (2002).
3. Yang, M. Z., Luo, J. L., Yang, Q., Qiao, L. J. & Norton, P. R. Effects of hydrogen on semiconductivity of passive films and corrosion behavior of 310 stainless steel. *J. Electrochem. Soc.* **146**, 2107–2112 (1999).
4. Yu, J. G., Luo, J. L. & Norton, P. R. Effects of hydrogen on the electronic properties and stability of the passive films on iron. *Appl. Surf. Sci.* **177**, 129–138 (2001).
5. Schmuki, P. & Bohni, H. Metastable pitting and semiconductive properties of passive films. *J. Electrochem. Soc.* **139**, 1908–1914 (1992).
6. Zeng, Y. M., Luo, J. L. & Norton, P. R. A study of semiconducting properties of hydrogen containing passive films. *Thin. Solid. Films.* **460**, 116–124 (2004).
7. Yang, Q. & Luo, J. L. Effects of hydrogen on disorder of passive films and pitting susceptibility of type 310 stainless steel. *J. Electrochem. Soc.* **148**, B29–B35 (2001).
8. Thomas, S., Sundararajan, G., White, P. & Birbilis, N. The effect of absorbed hydrogen on the corrosion of steels: Review, discussion and implications. *Corrosion* **73**, 426–436 (2017).
9. Malik, A., Ahmed, S. & Andijani, I. *Investigation on the Failure of Steel Welded Joints in Sea Water 1026–1027*. (Saline water conversion corporation, R&D, Saudi Arabia, 2014).
10. Chan, K. W. & Tjong, S. C. Effect of secondary phase precipitation on the corrosion behavior of duplex stainless steels. *Materials* **7**, 5268–5304 (2014).
11. Bhattacharya, A. *Stress Corrosion Cracking of Duplex Stainless Steels in Caustic Solutions*. (Georgia Institute of Technology, Atlanta, GA, USA, 2008). Ph.D. thesis.
12. Sato, N. & Sharma, S. K. *in Green Corrosion Chemistry and Engineering: Opportunities and Challenges* Ch. 1 (Wiley-VCH Verlag GmbH & Co. KGaA, Boschstr. 12, 69469 Weinheim, Germany, 2011).
13. Kim, J. S., Cho, E. A. & Kwon, H. S. Photoelectrochemical study on the passive film on Fe. *Corros. Sci.* **43**, 1403–1409 (2001).
14. Paola, A. D., Quarto, F. D. & Sunseri, C. A. Photoelectrochemical characterization of passive films on stainless steels. *Corros. Sci.* **26**, 935–948 (1986).
15. Yao, Y., Qiao, L. J. & Volinsky, A. A. Hydrogen effects on stainless steel passive film fracture studied by nanoindentation. *Corr. Sci.* **53**, 2679–2683 (2011).
16. Souier, T. & Chiesa, M. Effect of surface conditions and strain hardening on the passivity breakdown of 304 stainless steel. *J. Mater. Res.* **27**, 1580–1588 (2012).
17. Guo, L. Q., Lin, M. C., Qiao, L. J. & Volinsky, A. A. Duplex stainless steel passive film electrical properties studied by in situ current sensing atomic force microscopy. *Corros. Sci.* **78**, 55–62 (2014).
18. Guo, L. Q., Qin, S. X., Yang, B. J., Liang, D. & Qiao, L. J. Effect of hydrogen on semiconductive properties of passive film on ferrite and austenite phases in a duplex stainless steel. *Sci. Rep.* **7**, 3317 (2017).
19. Guo, L. Q., Lin, M. C., Qiao, L. J. & Volinsky, A. A. Ferrite and austenite phase identification in duplex stainless steel using SPM techniques. *Appl. Surf. Sci.* **287**, 499–501 (2013).
20. Garfias-Mesias, L. F., Skyes, J. M. & Tuck, C. D. S. The effect of phase compositions on the pitting corrosion of 25 Cr duplex stainless steel in chloride solutions. *Corros. Sci.* **38**, 1319–1330 (1996).
21. Guo, L. Q., Yang, B. & Qin, S. Relationship between hydrogen-induced phase transformations and pitting nucleation sites in duplex stainless steel. *Int. J. Mater. Res.* **107**, 109–113 (2016).
22. Owczarek, E. & Zakroczymski, T. Hydrogen transport in a duplex stainless steel. *Acta Mater.* **48**, 3059–3070 (2000).
23. Yu, J. G., Luo, J. L. & Norton, P. R. Investigation of hydrogen induced pitting active sites. *Electrochim. Acta* **47**, 4019–4025 (2002).
24. Guo, L. Q. et al. Effect of hydrogen on pitting susceptibility of 2507 duplex stainless steel. *Corr. Sci.* **70**, 140–144 (2013).
25. Li, M., Guo, L. Q., Qiao, L. J. & Bai, Y. The mechanism of hydrogen-induced pitting corrosion in duplex stainless steel studied by SKPFM. *Corr. Sci.* **60**, 76–81 (2012).
26. Guo, L. Q. et al. Effect of annealing temperature on the corrosion behavior of duplex stainless steel studied by in situ techniques. *Corros. Sci.* **53**, 3733–374 (2011).
27. Lantz, M. A., O'Shea, S. J. & Welland, M. E. Atomic-force-microscope study of contact area and friction on $NbSe_2$. *Phys. Rev. B* **55**, 10776 (1997).
28. Lantz, M. A., O'Shea, S. J. & Welland, M. E. Simultaneous force and conduction measurements in atomic force microscopy. *Phys. Rev. B* **56**, 15345 (1997).